Chapter 2
Cosmic Rays

A variety of different types of radiation reaches the Earth's atmosphere, covering many orders of magnitude in flux and energy: from very low energies below 10^{-3} eV, like the cosmic microwave background radiation [33], to the highest energies of charged cosmic ray particles with up to a few 10^{20} eV [36] (see Fig. 2.1). The extraterrestrial origin of cosmic rays was discovered by Victor Hess in 1912, when he measured an increase of ionizing radiation with height during balloon ascents [25]. Usually, the term 'cosmic rays' only refers to those particles coming from outside our solar system, i.e., particles with energies above $\sim 10^9$ eV. This cosmic radiation consists mainly of protons, but heavier atomic nuclei, electrons, positrons, anti-protons, gamma rays and neutrinos are also present. Sometimes, gamma rays and neutrinos do not count as cosmic rays, because the cosmic accelerators are believed to accelerate only charged particles, and thus any uncharged particle ought to be a secondary product of a charged primary cosmic ray particle. Even today, it is not totally clear what the sources of cosmic rays are and which mechanism is responsible for the acceleration of cosmic rays at the highest energies [14].

Since the flux of cosmic rays decreases rapidly with energy, different techniques are required to detect lower energy particles ($E \lesssim 10^{14}$ eV) and higher energy particles ($E \gtrsim 10^{13}$ eV). Lower energy cosmic rays can be measured directly with particle detectors on balloons or space craft. Higher energy cosmic rays are so rare that a detection with sufficient statistics needs larger detection areas than direct measurements can provide. Thus, indirect measurement methods are used, based on the detection of extensive air showers induced by cosmic rays. These air showers consist of secondary particles generated in the atmosphere when a primary cosmic ray particle interacts with air molecules. Air showers can be detected either by particle detectors on ground or by measuring electromagnetic radiation induced by the air shower particles in the atmosphere. The difficulty lies in the reconstruction of the primary cosmic ray particle properties, i.e., its arrival direction, energy and mass.

This chapter gives a short introduction to the current knowledge about the origin of cosmic rays, the development of air showers and the techniques to measure them. Special emphasis is given to the emission and detection of air shower induced radio

F. G. Schröder, *Instruments and Methods for the Radio Detection of High Energy Cosmic Rays*, Springer Theses, DOI: 10.1007/978-3-642-33660-7_2,

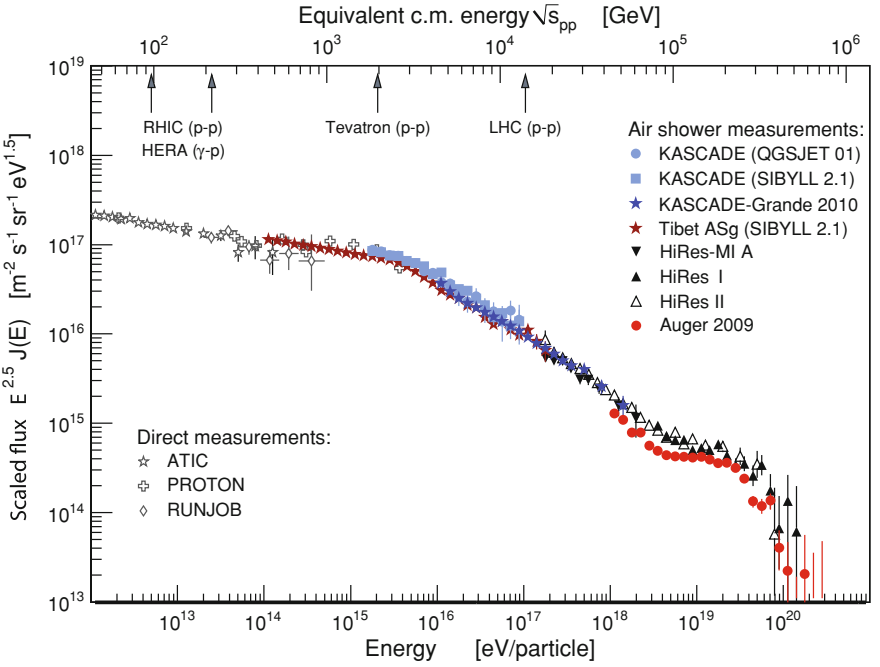

Fig. 2.1 Cosmic ray energy spectrum from exemplary chosen direct balloon and satellite experiments, and indirect air shower based measurements [14]

pulses—a relatively new and promising approach for cosmic ray detection at ultra high energies.

2.1 Origin of Cosmic Rays

The almost uniform power law of the cosmic ray energy spectrum indicates that the acceleration of primary particles is performed in a similar way at all energies, but not necessarily by the same type of source. A favored model is the relativistic shock front acceleration (first order Fermi acceleration) [13, 20]: When a relativistic particle is reflected by a shock front, it gains energy as the shock front is moving towards the particle (like a tennis ball is hit and reflected by a racket). Although existing shock fronts in space do not reflect particles instantaneously, but gradually by magnetic fields, the basic principle of acceleration holds true. Due to a certain probability for the particles to escape form the acceleration zone after each reflection at the shock front, a power law energy spectrum is generated. The power law index is predicted to be around -2, and thus slightly higher than the spectral index measured at Earth (-2.7 for $E \lesssim 10^{15}$ eV). But cosmic ray propagation models for the magnetic fields in the Milky Way and in intergalactic space can explain the observed discrepancy [16].

The question remains where to find the accelerating shock fronts. Galactic cosmic rays at lower energies ($\lesssim 10^{14}$ eV) originate at least partly from shock fronts generated by super nova explosions, so called super nova remnants. The evidence for this is threefold. First, the observation of gamma rays from super nova remnants with energies up to $\sim 10^{14}$ eV [4] proves that they can accelerate primary particles at least up to that energy, and probably to even higher energies because gamma rays are supposed to be emitted by accelerated charged particles or secondary pions. However, these charged primary particles might be predominantly electrons, and not or only partially nuclei. Second, the composition of galactic cosmic rays matches the expectations from models, which assume the acceleration taking place in OB associations [41]. These are regions of the Milky Way with a high rate of super novae explosions. Third, the energy output of super novae in our galaxy is sufficient to explain the observed flux of cosmic rays.

At higher energies, the situation is less clear. At the knee ($\sim 10^{15.7}$ eV), the slope of the cosmic ray energy spectrum steepens, since the flux of light nuclei decreases and the primary composition becomes heavier [7]. Hence, the knee could indicate the maximum energy reachable by super nova shock front acceleration. This picture gets additional support because at higher energies ($\sim 10^{17}$ eV), another kink in the spectrum is observed. It is at about 26 times the energy of the knee and could indicate the maximum energy for iron nuclei ($Z = 26$) reachable by super nova shock front acceleration [9]. A second explanation for this features would be the leakage of cosmic rays from our Milky Way, since the galactic magnetic fields might not be strong enough to bind them anymore at these energies. In both cases, it is likely that another type of source is responsible for cosmic rays at energies beyond $\sim 10^{17}$ eV.

In principle, a list of source candidates can be obtained by looking at the magnetic field strength B at a possible source and its extension L. The product BL indicates how long cosmic ray particle can remain in the accelerating source region. Hence, the size and magnetic field strength of a source candidate leads to a theoretical maximum energy which can be reached by any electromagnetic acceleration process. Such a candidate selection was first be done by Hillas [26], and yields several galactic and extra-galactic source candidates like neutron stars, gamma ray bursts, and active galactic nuclei (see Fig. 2.2). The transition energy from galactic to extra-galactic cosmic rays is not known, yet. It might be at the ankle, a flattening in the spectrum at $\sim 10^{18.3}$ eV.

From observations, it is only known that at least a part of the ultra high energy cosmic rays ($E \gtrsim 10^{19.6}$ eV) is coming from outside our galaxy, since the arrival direction of those cosmic rays are correlated with the distribution of nearby ($\lesssim 100$ Mpc) galaxies [2, 3]. This is consistent with expectations, as protons with higher energies should not be able to travel larger distances. This is because of the GZK cutoff [22, 47]: higher energy protons would interact with photons of the cosmic microwave background and loose energy. For heavier nuclei there exist similar, but slightly different cutoffs, e.g., due to photo dissociation [5].

Solving the open questions of ultra high energy cosmic ray physics, especially the question of their origin, requires accurate and precise measurements of the flux, energy, arrival direction and particle type (mass) of primary cosmic rays. Because the

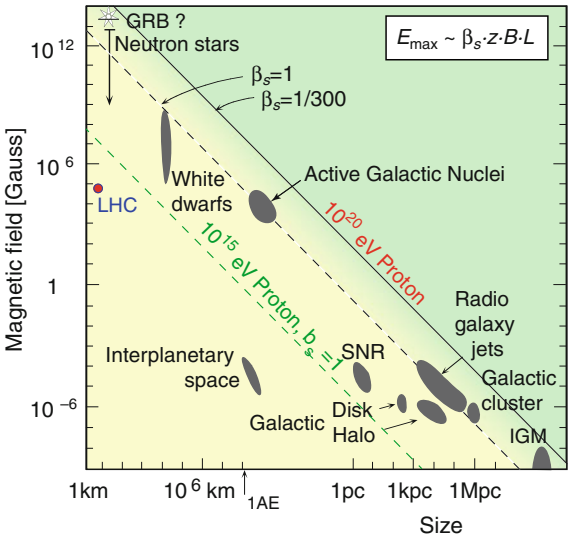

Fig. 2.2 Hillas plot of candidate sources for acceleration of ultra high energy cosmic rays [26] (adapted, with permission, from the Annual Review of Astronomy and Astrophysics, Vol. 22 © 1984 by Annual Reviews, www.annualreviews.org)

flux at the highest energies is extremely low, this can only be done by experiments with a large exposure, i.e., by huge air shower observatories like the Pierre Auger Observatory [1], or by future space craft observatories, like JEM-EUSO [45]. Moreover, systematic uncertainties demand a combination of several detection techniques to increase the measurement accuracy.

2.2 Cosmic Ray Air Showers

When ultra high energy cosmic rays hit the Earth's atmosphere they create particle air showers [12], similar to the particle showers known from calorimeters in high energy physics (see Fig. 2.3). Understanding the properties of air showers in detail requires simulations which can, for example, be accomplished with AIRES [44] or CORSIKA [24]. A primary particle of a certain energy, mass and incoming direction is assumed. Its interaction with the atmosphere as well as the interactions of all secondary particles are modeled with a Monte Carlo simulation. Since the relevant energy scale exceeds the range of accelerator experiments, measured cross-sections are extrapolated. Thus, air shower models and simulations can only approximately describe nature, with little, but significant deviations (see e.g., [6]). The basic features of air showers can already be understood without simulations, from simple phenomenological considerations. Such a phenomenological air shower model can be found in [38], for example. A summary is presented here.

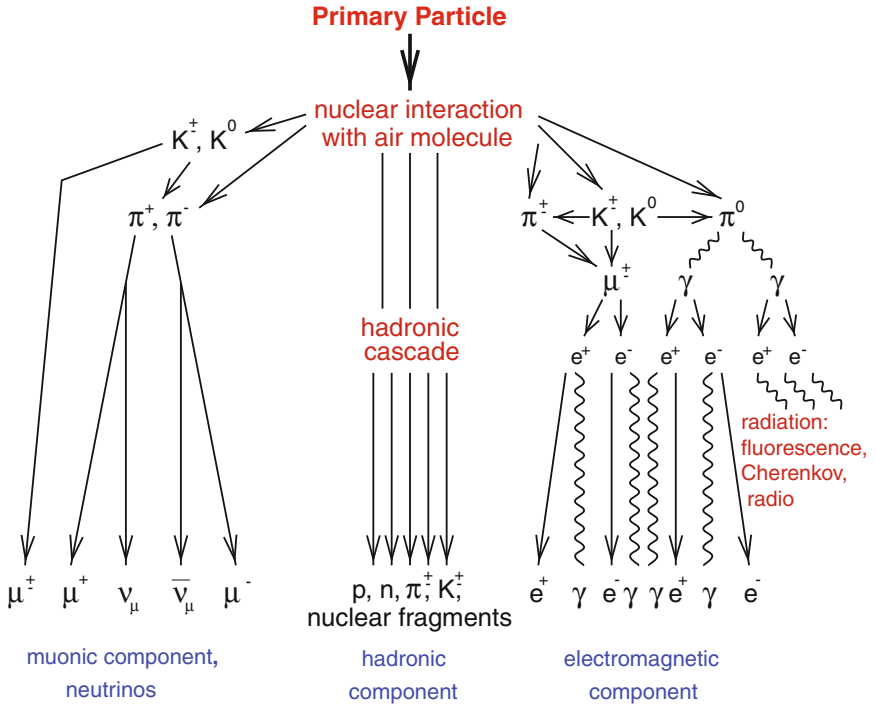

Fig. 2.3 Scheme of the development of an extensive air shower initiated by a cosmic ray nucleus (adapted from Ref. [23], with permission from IOP Publishing)

When the primary cosmic ray particle, e.g., a nucleus, scatters inelastically with an air nucleus, it generates secondary particles of different types, which interact themselves with other air nuclei. These interactions lead to electromagnetic or hadronic cascades, depending on the particle type. High energy gammas and electrons (or positrons) induce electromagnetic cascades. In a simple model, each photon creates an electron-positron-pair after a splitting length d, and each electron above a critical energy of about 85 MeV looses half its energy per splitting length d by radiating a photon ($d = \lambda_r \ln 2$ with the radiation length $\lambda_r \approx 37\,\mathrm{g/cm^2}$ in air). Electrons below the critical energy will be absorbed by the atmosphere.

Hadronic cascades are initiated by nuclei and hadrons. They interact with air nuclei and produce mainly mesons such as charged and uncharged pions, and kaons. In a simple model kaons are neglected, and in each interaction, one third of the energy is allotted to neutral pions, which decay immediately into photons and feed the electromagnetic cascade. The other two thirds of the energy are alloted to charged pions which will interact again after an interaction length of about $120\,\mathrm{g/cm^2}$ (in air), until the energy of the charged pions drops below $\sim$20 GeV. Then, the pions will decay into muons, before another interaction can take place. Because of their relativistic speed, most of the muons will reach the ground before decaying. The number and energy of hadrons reaching ground level is negligible for most practical purposes, except

for high altitudes or close to the shower axis. Thus, most experiments concentrate on measuring muons and electromagnetic particles.

The primary energy can be estimated from the electron and muon numbers N_e and N_μ at observation level: $E_0 \approx a \cdot (N_e + bN_\mu)$ at sea level, with a and b depending on the detection thresholds ($a = 0.85\,\text{GeV}$ and $b = 25$ in the simplified model without detection thresholds [38]). At primary energies of 10^{17} eV, about 90 % of the shower energy is in the electro magnetic cascade. Consequently, the primary energy can—within some uncertainties—be obtained by measuring alone the electromagnetic shower component.

The shower maximum X_{max} (g/cm^2) is the atmospheric depth, where the number of particles reaches its maximum. X_{max} is sensitive to the type of the primary particle because photons (and neutrinos) are assumed to interact on average more deeply in the atmosphere than nuclei. Moreover, X_{max} is even sensitive to the mass of the primary nuclei. In a simplified model, at high energies each nucleon is supposed to interact separately with atmospheric nuclei. Hence, at the same primary energy, heavier nuclei will on average interact earlier in the atmosphere, and give rise to fewer generations of secondary particles. Consequently, the muon number is increased with respect to proton showers by $N_\mu^A = N_\mu^p \cdot A^{0.15}$, and X_{max} is lower. Typical X_{max} values at primary energies of 10^{17} eV are 580 g/cm^2 for iron showers and 680 g/cm^2 for proton showers.

2.3 Classical Measurement Techniques for Air Showers

Classical measurement techniques for air showers rely either on particle detection on ground or indirect measurements of the energy content of the electromagnetic cascade, e.g., by observing fluorescence or Cherenkov light produced by the electrons when traveling through the atmosphere. As Cherenkov light measurements are important mainly for gamma ray observation at energies of $\sim$TeV, they are not discussed here. The detection of secondary particles on ground and fluorescence light are well established and successful techniques for cosmic ray measurements at ultra high energies. Their main advantages and disadvantages are presented in the following paragraphs (see also Table 2.1).

Detecting the secondary particles on ground requires large and expensive arrays of particle detectors, like scintillators or water Cherenkov counters. They have the advantage of a close to 100 % duty cycle and a relatively simple determination of the exposure, which is mandatory for evaluation of the cosmic ray flux at a certain energy. Furthermore, the arrival direction of the primary particle can easily be obtained from the relative particle arrival times at different detector stations. However, ground arrays have the disadvantage that they measure only one stage of the shower development, namely when the shower intersects the ground plane. The primary energy can be estimated from the total number of detected secondary particles and the primary mass from the ratio of electrons and muons. However, fluctuations in the shower development and extrapolations of the interaction models beyond the range probed by accelerator experiments lead to relatively large uncertainties.

Table 2.1 Performance comparison of different techniques for air shower measurement[a]: surface particle detectors (SD), fluorescence light detectors (FD) and digital radio arrays (RD)

	SD	FD	RD
Angular resolution	+	−/o [b]	+
Energy reconstruction accuracy	o[c]	+	o/+ [d]
Sensitivity to primary mass	−[c]	+	−/+ [d]
Determination of exposure	+	−	−
Duty cycle [e]	∼100 %	∼10 %	∼95 %
Energy threshold	$\sim 10^{14}$ eV	$\sim 10^{17}$ eV	$\sim 10^{17}$ eV

Legend: + good, o average, − poor

[a]This table reflects the author's personal view of how the different detection techniques compare with each other. The performances of surface detector arrays and fluorescence telescopes are intrinsically better when used in hybrid combination

[b]Mono/stereo mode; even better in hybrid combination

[c]Due to systematic uncertainties of air shower models

[d]Demonstrated, current status/expectation after further research, including detector development and better understanding of the radio emission mechanism

[e]Principal limit, e.g., due to light and weather conditions, not including down-time and maintenance

Fluorescence telescopes allow the detection of air showers in a large area by observing fluorescence light of nitrogen atoms excited by the electromagnetic cascade. The intensity of the fluorescence light is proportional to the primary energy within comparably small uncertainties. Furthermore, fluorescence measurements allow a precise determination of $X_{\max}$ (with $\Delta X_{\max} \sim 20\,\mathrm{g/cm^2}$). However, they have the big disadvantage that they are limited to dark, moonless nights resulting in a limited duty cycle of about 10 %. In addition, it is difficult to estimate the exposure because it is uncertain, up to which maximum distance an air shower at a specific energy can be seen.

Most of the disadvantages of both detection techniques can be overcome by combining them in a hybrid experiment. Consequently, two cosmic ray experiments of the latest generation, namely the Pierre-Auger-Observatory [1] and the Telescope Array [39], consist of fluorescence telescopes taking data simultaneously with a particle detector array. Still, even in these hybrid experiments, high quality data are limited by the low duty cycle of ∼10 % of fluorescence measurements. Thus, complementary detection methods with a higher duty cycle are explored, and one of the most promising is the detection of radio pulses emitted by air showers.

2.4 Radio Emission from Air Showers

The measurement of the radio emission of the electrons and positrons in an air shower is an alternative, and relatively new technique for cosmic ray detection. The principal features of the air shower induced radio emission have already been predicted [10, 35], and discovered about 50 years ago [34]. However radio detection of air showers became feasible only after the development of digital radio antenna arrays [19]. Since then, interest in this method has increased, and numerous researches

and developments are performed to explore the prospects of the radio technique for cosmic ray air shower detection.

The amplitude of the radio pulse is related to the number of particles and the energy of the electromagnetic cascade, which provides a calorimetric measurement of the primary energy, similar to the fluorescence method. By its sensitivity to the longitudinal shower development, measuring the radio emission should thus also provide a method for $X_{\max}$ determination, and hence, the type and mass of the primary particle (cf., Chap. 8). In addition, radio antenna arrays share two principal advantages of particle detector arrays: the arrival direction can be determined relatively simply by measurements of the pulse arrival times, and the duty cycle has no principle limitation. In fact, the duty cycle can reach almost 100 %, as recent experience shows that only periods with nearby thunderstorms and high atmospheric electric fields have to be excluded [17, 18], resulting in a realistic duty cycle of a few percent below that of particle detector arrays.

Nonetheless, there are some drawbacks. First, the detection threshold and the efficiency at a certain energy depend on the shower arrival direction, which makes a determination of the exposure and cosmic ray flux difficult, if radio antennas are not used in combination with a particle detector array. Second, it has still to be verified that the precision of primary energy and mass reconstruction can be as good as those of fluorescence measurements.

To overcome the current drawbacks and exploit the full potential of the radio detection technique, a detailed understanding of the emission process is mandatory. This is done by modeling the radio emission and comparing predictions of simulations with measurements. Furthermore, the performance of radio arrays can be cross-checked with coincident measurements in hybrid experiments. Whereas the current experimental situation is reviewed in the next chapter, the basic features of the radio emission and the status of our understanding of the emission process is summarized as follows.

2.4.1 Features of Air Shower Induced Radio Pulses

The radio emission of an air shower originates from the charged particles in the air shower, predominantly from the deflection of the electrons and positrons in the Earth's magnetic field. The emission is coherent if the thickness of the shower front (a few m) is smaller than the wavelength of the radio emission ($\widehat{=}$ radio frequencies $\lesssim$100 MHz). This leads to an amplification of the emission at those frequencies, and is the main reason why radio experiments operate typically below 80 MHz. Related to this frequency range is the time scale of the radio pulse which is in the order of 10 ns, depending on the lateral distance to the air shower axis (see Fig. 2.4).

The amplitude (field strength) of the radio pulse is proportional to the number of electrons in the air shower, i.e., roughly proportional to the primary energy—like it is expected for a coherent emission mechanism. Furthermore, the amplitude depends on the geomagnetic angle (i.e., the angle between the air shower axis and the

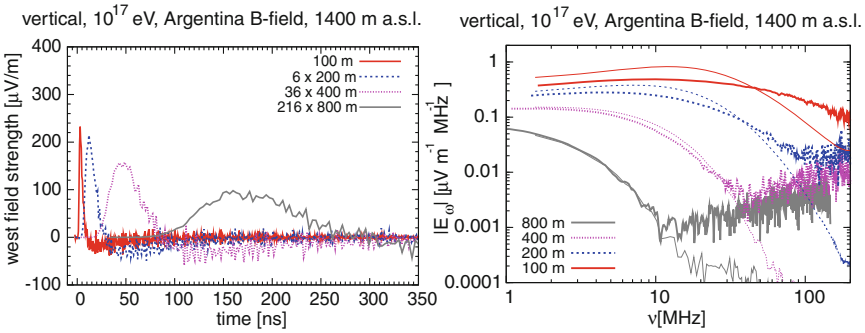

Fig. 2.4 Simulated radio emission for different lateral distances to the air shower axis (Reprinted from Ref. [31] with permission from Elsevier). *Left* REAS3 simulation of the east-west polarization component: unfiltered radio pulses. The bipolar structure of the radio pulses is only marginally visible due to numerical noise. *Right* REAS3 (*thick lines*) and MGMR (*thin lines*) simulations of the frequency spectrum. The rising field strength towards higher frequencies is an artifact of the numerical noise

Earth's magnetic field), the lateral distance and possibly the zenith angle. However, the details of those dependencies are not fully known and under investigation, e.g., by analyzing the lateral distribution of the radio signal (cf., [8], and Chap. 7).

Recently also the polarization of the radio signal became of interest. It is still being explored whether the polarization of the radio pulse can add valuable information to the reconstruction of the energy, mass and arrival direction of the primary particle. Several experiments measure, in addition to the arrival time and amplitude of radio pulses, their polarization, because this information at least helps to understand the emission process.

2.4.2 Emission Mechanisms

The radio emission of air showers is a complex phenomenon. It is predominantly of geomagnetic origin, but also other mechanisms contribute to the total emission. It should be noted that splitting the total radio emission into contributions by different emission mechanisms will only be an approximation to nature. The most realistic description of the radio emission is obtained when the complete electromagnetic emission is calculated as a whole, e.g., by an end-point formalism [32]. This approach is followed by the Monte Carlo simulation program REAS3 [37], the latest version of REAS [29, 30].

Nevertheless, studying different emission mechanisms separately can help to understand the physical processes at work. Summing up the emission of individual mechanisms is an approach followed by the MGMR [42] model. This model agrees in first order with REAS3 calculations [31], which shows that the picture of individual emission mechanisms is a reasonable approximation. The deviation

between REAS3 and MGRM is about a factor of 2–3. It is currently under investigation up to which degree this deviation is due to the approach or its implementation, e.g., the simplified air shower model used in MGMR.

The following overview gives a summary of different emission mechanisms contributing to the total radio emission. Current experimental results are compatible with contributions from all mechanisms, as long as the dominant component is of geomagnetic origin.

1. Transverse currents due to the Earth's magnetic field [35]:
   The (relativistic) electrons and positrons in the air shower experience a Lorentz force due to the Earth's magnetic field, and are separated from each other. This induces transverse currents in the air shower. Thus, the shower emits electromagnetic radiation, which happens to be predominantly in the range of radio waves below a few 100 MHz (see Fig. 2.4). Today, it is assumed that this is the major contribution to the total radio emission by air showers [31]. The polarization of any geomagnetic radio emission is perpendicular to the Earth's magnetic field, i.e., mainly in the east-west direction.
2. Variation of the dipole strength of the air shower [46]:
   The transverse currents in an air shower result in an electric dipole whose strength changes during the shower development. This leads to a radio emission, as if the shower were an emitting dipole antenna. Furthermore, the atmosphere transversed by the air shower is charged which should cause an additional, but smaller dipole-like radio emission [43].
3. Geosynchrotron effect [28]:
   The electrons and positrons in their air shower are not only separated by the Earth's magnetic field, but also accelerated, i.e., they change their momentum. This should result in a synchrotron-like geomagnetic radio emission, because the tracks of the electrons and positrons are curved. However, recent theoretical studies revealed that this is only a minor contribution [31], and it is still under investigation by which degree it influences the total radio emission by air showers.
4. Variation of the net charge excess (Askaryan effect [10]):
   In air showers, the number of electrons exceeds the number of positrons because of anti-particle absorption. The absolute amount of this charge excess changes during the shower development, as the total number of particles changes. Hence, this leads to a radio emission with radial polarization, like it is expected from any changing net charge (see also [31, 42]).
5. Cherenkov emission [11]:
   When a charge is traveling in a medium faster than the speed of light in this medium, it is emitting Cerenkov radiation. Thus, also in air showers Cherenkov emission should occur, since the positive and negative charges in the shower are separated, and there are more electrons than positrons. Sometimes this Cherenkov-like radio emission is also referred to as Askaryan emission, since it is easy to confound and not well separated from the emission due to the net charge variation in the shower [32]. However, Cherenkov-like emission can only take place in media with a refractive index $n > 1$. Thus, it could predominantly

be of importance for particle showers in dense media. However, it is not clear, whether Cherenkov emission is negligible against the Askaryan effect which also occurs at $n = 1$. Until now, radio emission in dense media has only been observed for accelerator beam induced showers.

6. Atmospheric electric fields:
   Not only magnetic, but also electric fields in the atmosphere can accelerate the charged particles of the air shower and lead to an additional radio emission. During thunderstorm conditions ($E_{\text{atm}} \sim 10000\,\text{V/m}$), this emission can be even stronger than the geomagnetic one [15]. It has still a measurable effect when the atmospheric electric field at ground reaches a strength of a few 1000 V/m [17]. So far, no influence has been detected under normal weather conditions ($E_{\text{atm}} \sim 100\,\text{V/m}$).
7. Molecular bremsstrahlung:
   Recently also radio emission by molecular bremsstrahlung is investigated. Laboratory experiments with particle showers induced by an accelerator beam measured a partially coherent radio emission at GHz frequencies [21]. Thus, several experiments have started to search for air shower emission in the GHz range. If successful, this technique would have the advantage that air showers could be detected at large lateral distances, because molecular bremsstrahlung is emitted isotropically, and not mainly in forward direction like the geomagnetic emission. It is not yet clear, whether molecular bremsstrahlung has any significant influence on the radio emission at MHz frequencies.

All emission processes are coherent at MHz frequencies because of the limited thickness of the air shower particle front (a few meters). Indeed, LOPES measurements show that the field strength of the radio pulse is (within errors) proportional to the primary energy [27], which proves that the emission is, at least to a large extent, coherent. Thus, any incoherent emission mechanisms can only play a minor role at LOPES energies ($\sim 10^{17}$ eV).

At the moment, the research on the radio emission processes is focusing on the attempt to understand the radio emission as a whole, respectively, to figure out to which degree each of the mechanisms is contributing. This can be determined by studying properties of the radio pulses (e.g., pulse shape, polarization and lateral distribution) and their dependencies on different shower parameters (e.g., the geomagnetic angle, azimuth and zenith). Another way to disentangle the details of the emission process is to compare data with simulations based on certain models. If a model includes all of the processes leading to radio emission, its predictions should match the measured data. Great progress was recently made since it has become possible to compare the measured radio field strength for each LOPES event with predictions of REAS simulations [40].

To test improved simulations like REAS3, and to study also minor contributions to the radio emission, experiments must develop an increased level of precision. The present thesis covers several techniques required for precise measurements, for instance time calibration (see Chap. 4), and noise treatment (see Chap. 6). The success of the improved experimental techniques and the revised models becomes

clear in the studies described in Chap. 7. For the first time, a simulation can predict measured radio data more or less correctly: lateral distributions of the radio field strength predicted by REAS3 are close to LOPES data. This gives rise to optimism that a detailed understanding of the air shower radio emission comes within reach.

References

1. J. Abraham et al. - Pierre Auger Observatory. Properties and performance of the prototype instrument for the Pierre Auger Observatory. *Nuclear Instruments and Methods in Physics Research A*, 523(1–2):50–95, 2004.
2. J. Abraham et al. - Pierre Auger Observatory. Anisotropy studies around the galactic centre at EeV energies with the Auger Observatory. *Astroparticle Physics*, 27:244–253, 2007.
3. P. Abreu et al. - Pierre Auger Observatory. Update on the correlation of the highest energy cosmic rays with nearby extragalactic matter. *Astroparticle Physics*, 34:314–326, 2010.
4. F. Aharonian et al. - H.E.S.S. Collaboration. Primary particle acceleration above 100 TeV in the shell-type supernova remnant RX J1713.7-3946h deep HESS observations. *Astronomy & Astrophysics*, 464(1):235–243, 2007.
5. D. Allard, E. Parizot, A.V. Olinto, et al. UHE nuclei propagation and the interpretation of the ankle in the cosmic-ray spectrum. *Astronomy & Astrophysics*, 443(3):L29–L32, 2005.
6. W. D. Apel et al. - KASCADE Collaboration. Test of interaction models up to 40 PeV by studying hadronic cores of EAS. *Journal of Physics G: Nuclear and Particle Physics*, 34(12):2581, 2007.
7. W. D. Apel et al. - KASCADE Collaboration. Energy spectra of elemental groups of cosmic rays: Update on the KASCADE unfolding analysis. *Astroparticle Physics*, 31(2):86–91, 2009.
8. W. D. Apel et al. - LOPES Collaboration. Lateral distribution of the radio signal in extensive air showers measured with LOPES. *Astroparticle Physics*, 32:294–303, 2010.
9. W. D. Apel et al. - KASCADE-Grande Collaboration. The spectrum of high-energy cosmic rays measured with KASCADE-Grande. *Astroparticle Physics*, 36:183–194, 2012.
10. G. A. Askaryan. Excess negative charge of an electron-photon shower and its coherent radio emission. *Soviet Physics JETP*, 14:441, 1962.
11. G. A. Askaryan. Coherent radio emission from cosmic showers in air and in dense media. *Soviet Physics JETP*, 21:658, 1965.
12. P. Auger, P. Ehrenfest, R. Maze, et al. Extensive Cosmic-Ray Showers. *Reviews of Modern Physics*, 11:288–291, 1939.
13. W. Axford et al. In *Proceedings of the 15th ICRC, Plovidv, Bulgaria*, volume 11, page 132, 1977.
14. J. Blümer, R. Engel, and J. R. Hörandel. Cosmic rays from the knee to the highest energies. *Progress in Particle and Nuclear Physics*, 63:293–338, 2009.
15. S. Buitink et al. - LOPES Collaboration. Amplified radio emission from cosmic ray air showers in thunderstorms. *Astronomy & Astrophysics*, 467:385–394, 2007.
16. R. Cowsik and L.W. Wilson. In *Proceedings of the 13th ICRC, Denver, USA*, volume 1, page 500, 1973.
17. M. Ender. Radiodetektion von Luftschauern unter dem Einfluss starker elektrischer Felder in der Atmosphäre. FZKA Report 7506, Forschungszentrum Karlsruhe, 2009.
18. M. Ender et al. - LOPES Collaboration. Radio Emission of Extensive Air Showers during Thunderstorms. In *Proceedings of the 31st ICRC, Łódź, Poland*, number 0405, 2009. http://icrc2009.uni.lodz.pl/proc/html/.
19. H. Falcke et al. - LOPES Collaboration. Detection and imaging of atmospheric radio flashes from cosmic ray air showers. *Nature*, 435:313–316, 2005.
20. E. Fermi. On the Origin of Cosmic Radiation. *Physical Review*, 75(8):1169, 1949.

21. P. W. Gorham et al. - WMAP. Observations of microwave continuum emission from air shower plasmas. *Physical Review D*, 78(3):032007, 2008.
22. K. Greisen. End to the Cosmic-Ray Spectrum? *Physical Review Letters*, 16:748–750, 1966.
23. A. Haungs, H. Rebel, M. Roth. Energy spectrum and mass composition of high-energy cosmic rays. *Reports on Progress in Physics*, 66(7):1145, 2003. http://dx.doi.org/10.1088/0034-4885/66/7/202.
24. D. Heck, J. Knapp, J. N. Capdevielle, et al. CORSIKA: A Monte Carlo Code to Simulate Extensive Air Showers. FZKA Report 6019, Forschungszentrum Karlsruhe, 1998.
25. V. F. Hess. Über Beobachtungen der durchdringenden Strahlung bei sieben Freiballonfahrt. *Physikalische Zeitschrift*, 13:1084, 1912.
26. A. M. Hillas. The Origin of Ultra-High-Energy Cosmic Rays. *Annual Review of Astronomy and Astrophysics*, 22:425–444, 1984.
27. A. Horneffer et al. - LOPES Collaboration. Primary Particle Energy Calibration of the EAS Radio Pulse Height. In *Proceedings of the 30th ICRC, Merida, Mexico*, volume 4, pages 83–86, 2007.
28. T. Huege and H. Falcke. Radio emission from cosmic ray air showers. Coherent geosynchrotron radiation. *Astronomy & Astrophysics*, 412:19–34, 2003.
29. T. Huege and H. Falcke. Radio emission from cosmic ray air showers. Monte Carlo simulations. *Astronomy & Astrophysics*, 430:779–798, 2005.
30. T. Huege and H. Falcke. Radio emission from cosmic ray air showers: Simulation results and parametrization. *Astroparticle Physics*, 24:116, 2005.
31. T. Huege, M. Ludwig, O. Scholten, and K.D. de Vries. The convergence of EAS radio emission models and a detailed comparison of REAS3 and MGMR simulations. *Nuclear Instruments and Methods in Physics Research Section A: Accelerators, Spectrometers, Detectors and Associated Equipment*, 662(Supplement 1):S179–S186, 2012. ARENA 2010.
32. C. W. James, H. Falcke, T. Huege, and M. Ludwig. General description of electromagnetic radiation processes based on instantaneous charge acceleration in "endpoints". *Physical Review E*, 84:056602, 2011.
33. N. Jarosik et al. - WMAP. Seven-Year Wilkinson Microwave Anisotropy Probe (WMAP) Observations: Sky Maps, Systematic Errors, and Basic Results. *ArXiv e-prints*, 2010. astro-ph/1001.4744.
34. J. V. Jelley, J. H. Fruin, N. A. Porter, et al. Radio Pulses from Extensive Cosmic-Ray Air Showers. *Nature*, 205:327–328, 1965.
35. F. D. Kahn and I. Lerche. Radiation from cosmic ray air showers. In *Proceedings of the Royal Society of London. Series A, Mathematical and Physical Sciences*, volume 289, page 206, 1966.
36. J. Linsley. Evidence for a Primary Cosmic-Ray Particle with Energy 10^{20} eV. *Physical Review Letters*, 10(4):146–148, 1963.
37. M. Ludwig and T. Huege. REAS3: Monte Carlo simulations of radio emission from cosmic ray air showers using an 'end-point' formalism. *Astroparticle Physics*, 34(6):438–446, 2011.
38. J. N. Matthews. A Heitler model of extensive air showers. *Astroparticle Physics*, 22:387–397, 2005.
39. J. N. Matthews et al. for the Telescope Array Collaboration. Overview of the Telescope Array Experiment. In *Proceedings of the 31st ICRC, Łódź, Poland*, number 1386, 2009. http://icrc2009.uni.lodz.pl/proc/html/.
40. S. Nehls. Calibrated Measurements of the Radio Emission of Cosmic Ray Air Showers. FZKA Report 7440, Forschungszentrum Karlsruhe, 2008.
41. B. F. Rauch et al. - TIGER Collaboration. Cosmic Ray origin in OB Associations and Preferential Acceleration of Refractory Elements: Evidence from Abundances of Elements $_{26}$Fe through $_{34}$Se. *Astrophysical Journal*, 697:2083–2088, 2009.
42. O. Scholten, K. Werner, and F. Rusydi. A macroscopic description of coherent geo-magnetic radiation from cosmic-ray air showers. *Astroparticle Physics*, 29:94–103, 2008.
43. O. Scholten, K. D. de Vries, and K. Werner. Coherent radiation from extensive air showers. *Nuclear Instruments and Methods in Physics Research Section A: Accelerators, Spectrometers, Detectors and Associated Equipment*, 662(Supplement 1):S80–S84, 2012. ARENA 2010.

44. S. J. Sciutto. AIRES: A system for air shower simulations (Version 2.2.0). *ArXiv Astrophysics e-prints*, 1999. astro-ph/9911331.
45. Y. Takahashi et al. - EUSO Collaboration. Science Objectives of the JEM EUSO mission on International Space Station. In *Proceedings of the 30th ICRC, Merida, Mexico*, 2007.
46. K. Werner and O. Scholten. Macroscopic Treatment of Radio Emission from Cosmic Ray Air Showers based on Shower Simulations. *Astroparticle Physics*, 29:393–411, 2008.
47. G. T. Zatsepin and V. A. Kuzmin. Upper limit of the spectrum of cosmic rays. *ZhETF Pis ma Redaktsiiu*, 4(3):114–117, 1966.

http://www.springer.com/978-3-642-33659-1

Instruments and Methods for the Radio Detection of High Energy Cosmic Rays

Schröder, F.

2012, XVIII, 190 p., Hardcover
ISBN: 978-3-642-33659-1